

Variants in the degron of *AFF3* are associated with intellectual disability, mesomelic dysplasia, horseshoe kidney, and epileptic encephalopathy

Norine Voisin,¹ Rhonda E. Schnur,^{2,3} Sofia Douzgov,^{4,5} Susan M. Hiatt,⁶ Cecilie F. Rustad,⁷ Natasha J. Brown,^{8,9,10} Dawn L. Earl,¹¹ Boris Keren,¹² Olga Levchenko,¹³ Sinje Geuer,^{14,15,43} Sarah Verheyen,¹⁶ Diana Johnson,¹⁷ Yuri A. Zarate,¹⁸ Miroslava Hančárová,¹⁹ David J. Amor,^{9,10} E. Martina Bebin,²⁰ Jasmin Blatterer,¹⁶ Alfredo Brusco,^{21,22} Gerarda Cappuccio,^{23,24} Joel Charrow,²⁵ Nicolas Chatron,^{1,26} Gregory M. Cooper,⁶ Thomas Courtin,¹² Elena Dadali,¹³ Julien Delafontaine,²⁸ Ennio Del Giudice,²³ Martine Doco,²⁹ Ganka Douglas,² Astrid Eisenkölbl,³⁰ Tara Funari,² Giuliana Giannuzzi,^{1,45} Ursula Gruber-Sedlmayr,³¹ Nicolas Guex,^{1,27} Delphine Heron,¹² Øystein L. Holla,³² Anna C.E. Hurst,³³ Jane Juusola,² David Kronn,³⁴ Alexander Lavrov,¹³ Crystle Lee,⁸ Séverine Lorrain,^{1,35} Else Merckoll,³⁶ Anna Mikhaleva,¹ Jennifer Norman,³⁷ Sylvain Pradervand,^{1,38} Darina Prchalová,¹⁹ Lindsay Rhodes,² Victoria R. Sanders,²⁵ Zdeněk Sedláček,¹⁹ Heidelis A. Seebacher,¹⁶ Elizabeth A. Sellars,¹⁸ Fabio Sirchia,^{38,46} Toshiki Takenouchi,³⁹ Akemi J. Tanaka,^{40,41} Heidi Taska-Tench,²⁵

(Author list continued on next page)

Summary

The ALF transcription factor paralogs, *AFF1*, *AFF2*, *AFF3*, and *AFF4*, are components of the transcriptional super elongation complex that regulates expression of genes involved in neurogenesis and development. We describe an autosomal dominant disorder associated with *de novo* missense variants in the degron of *AFF3*, a nine amino acid sequence important for its binding to ubiquitin ligase, or with *de novo* deletions of this region. The sixteen affected individuals we identified, along with two previously reported individuals, present with a recognizable pattern of anomalies, which we named KINSSHIP syndrome (KI for horseshoe kidney, NS for Nievergelt/Savarirayan type of mesomelic dysplasia, S for seizures, H for hypertrichosis, I for intellectual disability, and P for pulmonary involvement), partially overlapping the *AFF4*-associated CHOPS syndrome. Whereas homozygous *Aff3* knockout mice display skeletal anomalies, kidney defects, brain malformations, and neurological anomalies, knockin animals modeling one of the microdeletions and the most common of the missense variants identified in affected individuals presented with lower mesomelic limb deformities like KINSSHIP-affected individuals and early lethality, respectively. Overexpression of *AFF3* in zebrafish resulted in body axis anomalies, providing some support for the pathological effect of increased amount of *AFF3*. The only partial phenotypic overlap of *AFF3*- and *AFF4*-associated syndromes and the previously published transcriptome analyses of ALF transcription factors suggest that these factors are not redundant and each contributes uniquely to proper development.

Introduction

AFF1 (AF4/FMR2 family member 1 [*AF4*] [MIM: 159557]), *AFF2* (*FMR2* [MIM: 300806]), *AFF3* (*LAF4* [MIM: 601464]),

and *AFF4* (MIM: 604417) encode members of the ALF (AF4/LAF4/FMR2) family. These transcription factors share five highly conserved domains starting from the amino terminus: (1) an N-terminal homology domain (NHD); (2) the

¹Center for Integrative Genomics, University of Lausanne, Lausanne 1015, Switzerland; ²GeneDx, Gaithersburg, MD 20877, USA; ³Cooper Medical School of Rowan University, Division of Genetics, Camden, NJ 08103, USA; ⁴Manchester Centre for Genomic Medicine, St Mary's Hospital, Manchester University Hospitals NHS Foundation Trust, Manchester Academic Health Sciences Centre, Manchester M13 9WL, UK; ⁵Division of Evolution and Genomic Sciences, School of Biological Sciences, University of Manchester, Manchester M13 9NT, UK; ⁶HudsonAlpha Institute for Biotechnology, Huntsville, AL 35806, USA; ⁷Department of Medical Genetics, Oslo University Hospital, 0424 Oslo, Norway; ⁸Victorian Clinical Genetics Services, Flemington Road, Parkville, VIC 3052, Australia; ⁹Murdoch Children's Research Institute, Flemington Road, Parkville, VIC 3052, Australia; ¹⁰Department of Paediatrics, University of Melbourne, Royal Children's Hospital, Flemington Road, Parkville, VIC 3052, Australia; ¹¹Seattle Children's, Seattle, WA 98105, USA; ¹²Department of Genetics, Pitié-Salpêtrière Hospital, Assistance Publique - Hôpitaux de Paris, Groupe de Recherche Clinique Déficience Intellectuelle et Autisme UPMC, Paris 75013, France; ¹³Research Centre for Medical Genetics, Moscow 115522, Russia; ¹⁴Max Planck Institute for Molecular Genetics, Berlin 14195, Germany; ¹⁵Institute for Medical and Human Genetics, Charité Universitätsmedizin Berlin, Berlin 10117, Germany; ¹⁶Institute of Human Genetics, Diagnostic and Research Center for Molecular Biomedicine, Medical University of Graz, 8010 Graz, Austria; ¹⁷Sheffield Clinical Genetics Service, Sheffield S10 2TQ, UK; ¹⁸Section of Genetics and Metabolism, University of Arkansas for Medical Sciences, Little Rock, AR 72701, USA; ¹⁹Charles University Second Faculty of Medicine and University Hospital Motol, 150 06 Prague, Czech Republic; ²⁰Department of Neurology, University of Alabama at Birmingham, Birmingham, AL 35294, USA; ²¹Department of Medical Sciences, University of Torino, Torino 10126, Italy; ²²Medical Genetics Unit, Città della Salute e della Scienza University Hospital, Torino 10126, Italy; ²³Department of Translational Medicine, Section of Pediatrics, Federico II University, Naples 80131, Italy; ²⁴Telethon Institute of Genetics and Medicine, Pozzuoli, Naples 80078, Italy; ²⁵Division of Genetics, Birth Defects & Metabolism, Ann & Robert H. Lurie Children's Hospital of Chicago, Chicago, IL 60611, USA; ²⁶Genetics Department, Lyon University Hospital, Lyon 69007, France; ²⁷Bioinformatics

(Affiliations continued on next page)



Elin Tønne,⁷ Kristian Tveten,³² Giuseppina Vitiello,²³ Markéta Vlčková,¹⁹ Tomoko Uehara,³⁹ Caroline Nava,¹² Binnaz Yalcin,^{1,42,44} Kenjiro Kosaki,³⁹ Dian Donnai,^{4,5} Stefan Mundlos,^{14,15} Nicola Brunetti-Pierri,^{23,24} Wendy K. Chung,^{40,41} and Alexandre Reymond^{1,*}

hallmark ALF domain, which interacts with seven in absentia homolog (SIAH) ubiquitin ligases through the [xPxAxVxPx] degron motif^{1,2} and thus regulates protein degradation mediated by the proteasome pathway; (3) a serine-rich transactivation domain;³ (4) a bipartite nuclear localization sequence (NLS); and (5) an eight helices C-terminal homology domain (CHD) that mediates homo- or heterodimerization of AFFs.^{4–6} *AFF1*, *AFF3*, and *AFF4* have each been identified as fusion partners of the mixed-lineage leukemia *KMT2A* gene (MIM: 159555) involved in acute pediatric leukemias.³ They are part of the super elongation complex⁷ implicated in transcription of a set of genes, among them histones, retinoid signaling, and *HOX* genes involved in neurogenesis and several other developmental processes (e.g., *Hoxa1*, *Cdx11*, and *Cyp26a1*^{7,8}). Mutations of the fruit fly ALF orthologous gene *lilliputian* (*lilli*) were shown to prevent neuronal differentiation and to decrease cell growth and size.^{9,10} Silencing of *AFF2* by CGG repeat expansion is associated with the FRAXE intellectual disability syndrome¹¹ (MIM: 309548), whereas hypermethylation of a mosaic CGG repeat expansion in the promoter of *AFF3*, which leads to its silencing in the central nervous system, was associated with a cytogenetic fragile site (*FRA2A*) and intellectual disability in three families.¹² *AFF3* is also known for regulating the expression of imprinted genes^{13,14} such as *XIST* (MIM: 314670) through binding to differentially methylated regions.¹⁵ Individuals with either a *de novo* missense variant or a 500 kb microdeletion within the *AFF3* locus and presenting with mesomelic dysplasia and skeletal dysplasia and encephalopathy, respectively, were described.^{16,17}

De novo missense variants in *AFF4* have been linked with CHOPS (cognitive impairment and coarse facies, heart defects, obesity, pulmonary problems, short stature, and skeletal dysplasia) syndrome^{18,19} (MIM: 616368). These variants were suggested to act through reduced clearance of *AFF4* by *SIAH1* (MIM: 602212), a hypothesis supported by surviving adult *Aff4*-null mice, which have only azoospermia and no features of CHOPS syndrome. However, a

majority of *Aff4*^{-/-} embryos died *in utero* with severely shrunken lung alveoli.²⁰ Upregulation of *AFF4* resulted in dysregulation of genes involved in skeletal development and anterior/posterior pattern formation such as *MYC* (MIM: 190080), *JUN* (MIM: 165160), *TMEM100* (MIM: 616334), *ZNF711* (MIM: 314990), and *FAM13C*.¹⁸ These changes were proposed to impair complex functions leading to cohesinopathies associated with the clinical phenotypes seen in the eleven reported individuals with CHOPS and in Cornelia de Lange syndrome (CdLS [MIM:122470]).^{18,19}

Here, we describe 16 individuals with either *de novo* missense (15) or deletion variants in *AFF3* and a recognizable pattern of anomalies, including developmental delay, intellectual disability, seizures, dysmorphic facial features, mesomelic dysplasia, horseshoe or hypoplastic kidney, and failure to thrive, and compare them to previously published individuals with *AFF3* or *AFF4* mutations. Although there is some overlap, the clinical presentation of this *AFF3*-associated autosomal dominant disorder appears to be distinct from CHOPS syndrome.

Material and methods

Enrollment

Participants were enrolled after written informed consent was obtained from parents or legal guardians according to ethical review boards' policies. The clinical evaluation included medical history interviews, physical examinations, and review of medical records. The Deciphering Developmental Disorders (DDD)²¹ identifier of proband 8 is DDD276869.

Exome and genome sequencing and analysis

Affected individuals were selected for sequencing to establish a diagnosis.

Proband 1

Exome sequencing of the family trio was performed on a NovaSeq Sequencing System (Illumina, San Diego, CA) after a 5-plex enrichment with a SeqCap EZ MedExome Kit (Roche, Basel, Switzerland)

Competence Center, University of Lausanne, Lausanne 1015, Switzerland; ²⁸Swiss Institute of Bioinformatics, Lausanne 1015, Switzerland; ²⁹Secteur Génétique, CHU Reims, EA3801, SFR CAPSANTE, 51092 Reims, France; ³⁰Department of Pediatrics and Adolescent Medicine, Johannes Kepler University, Kepler University Hospital Linz, Krankenhausstraße 26-30, 4020 Linz, Austria; ³¹Division of General Pediatrics, Department of Pediatrics and Adolescent Medicine, Medical University of Graz, 8036 Graz, Austria; ³²Department of Medical Genetics, Telemark Hospital Trust, 3710 Skien, Norway; ³³Department of Genetics, University of Alabama at Birmingham, Birmingham, AL 35233, USA; ³⁴New York Medical College, Valhalla, NY 10595, USA; ³⁵Protein Analysis Facility, University of Lausanne, Lausanne 1015, Switzerland; ³⁶Department of Radiology, Oslo University Hospital, 0424 Oslo, Norway; ³⁷Integrative Pediatric Neurology, Oklahoma City, OK 73112, USA; ³⁸Institute for Maternal and Child Health - IRCCS Burlo Garofolo, Trieste 34100, Italy; ³⁹Center for Medical Genetics, Department of Pediatrics, Keio University School of Medicine, Tokyo 1608582, Japan; ⁴⁰Department of Pediatrics, Columbia University, New York, NY 10032, USA; ⁴¹Department of Medicine, Columbia University, New York, NY 10032, USA; ⁴²Institut de Génétique et de Biologie Moléculaire et Cellulaire, Illkirch 67404, France

⁴³Present address: Center for Human Genetics, Bioscientia, Ingelheim 55218, Germany

⁴⁴Present address: Inserm UMR1231, University of Bourgogne Franche-Comté, 21000 Dijon, France

⁴⁵Present address: Department of Biosciences, University of Milan, 20133 Milan, Italy; Institute of Biomedical Technologies, National Research Council, 20054 Segrate (Milan), Italy

⁴⁶Present address: Department of Molecular Medicine, University of Pavia, 27100 Pavia, Italy

*Correspondence: alexandre.reymond@unil.ch
<https://doi.org/10.1016/j.ajhg.2021.04.001>

according to manufacturer's specifications. Reads were mapped with Novoalign (v.4.02.02), sorted, and indexed in a bam file (picard-tools-1.129 and samtools-0.1.19). Duplicates were flagged and coverage was calculated (picard-tools-1.129). Variant calling was performed with the GATK 3.7 Haplotype Caller. Variants were then filtered (bcftools-1.2) and annotated with snpEff 4.3T, the Genome Aggregation Database (gnomAD), ClinVar, and an in-house variant database.

Probands 2 and 3

Trio exome analysis was performed on a NextSeq 500 Sequencing System (Illumina, San Diego, CA) after a 12-plex enrichment with a SeqCap EZ MedExome Kit (Roche, Basel, Switzerland) according to manufacturer's specifications. Sequence quality was assessed with FastQC 0.11.5; reads were mapped with BWA-MEM (v.0.7.13), sorted, and indexed in a bam file (samtools 1.4.1); duplicates were flagged (sambamba 0.6.6); and coverage was calculated (picard-tools 2.10.10). Variant calling was done with the GATK 3.7 Haplotype Caller. Variants were then annotated with SnpEff 4.3, dbNSFP 2.9.3, gnomAD, ClinVar, Human Gene Mutation Database (HGMD), and an internal database. Coverage for these samples was 93% at a 20× depth threshold.

Probands 4 and 15

Exomes were captured via the Integrated DNA Technologies (IDT) xGen Exome Research Panel v.1.0. Sequencing and analyses were performed as previously described.²² The general assertion criteria for variant classification are publicly available on the GeneDx ClinVar submission page.

Proband 5

A Nextera DNA Flex Library Prep Kit was used for library preparation. Sequencing was performed on a NextSeq 550 (Illumina) and data were analyzed, including filtering and prioritization, with HPO terms (HP: 0001250, HP: 0011344, HP: 0001252, HP: 0000639, HP: 0000085, HP: 0001776, HP: 0002079, HP: 0010609, HP: 0001081, HP: 0009811, and HP: 0001508) with the VarSeq software (Golden Helix). Sanger sequencing confirmed the *de novo* status of the variant.

Proband 6

The exomes of proband 6 and his parents were sequenced in the frame of the DDD study²¹ and confirmed by the 100k Genomes Project.

Proband 7

The exomes of proband 7, his parents, and two healthy siblings were captured and sequenced as described.²³ Variants were called and filtered with the Varapp software.²⁴ Sanger sequencing confirmed the anticipated segregation of the potentially causative variants.

Proband 8

Exome capture and sequencing was performed as previously described.²¹

Proband 9

Exome sequencing of proband 9 was performed as previously described.²⁵ Sanger sequencing of samples from parents revealed *de novo* segregation of the variant.

Proband 10

Trio genome analysis was performed as previously described.²⁶ Sanger sequencing confirmed the *de novo* variant reported here.

Proband 11

Trio exome analysis was performed as previously described.²⁷

Proband 12

Sample preparation and enrichment was performed with a TruSeq DNA Exome Kit (Illumina), and sequencing was performed via NextSeq 500 (Illumina) with mean region coverage of 83×.

Variants were called with VarAFT software. Variant analysis was performed according to standards and guidelines for the interpretation of sequence variants.²⁸ Sanger sequencing confirmed the *de novo* origin of the variant.

Proband 13

Trio exome analysis was performed with Agilent SureSelect CRE exome capture, Illumina NextSeq 500 sequencer, and a mean coverage of 100×. Data were processed with Cpipeline,²⁹ and variant filtering and prioritization were phenotype driven (gene lists: intellectual disability, Mendeliome). Variant classification followed ACMG (the American College of Medical Genetics and Genomics) guidelines.

Proband 14

Trio exome analysis was performed with a Nextera Rapid Capture Exome Enrichment Kit and Nextera DNA Flex Library Prep Kit and sequenced on a NextSeq 550 (all Illumina), and data were analyzed, including filtering and prioritization, via HPO terms (HP: 0004879, HP: 0001263, HP: 0004324, and HP: 0000098) with the VarSeq software (Golden Helix).

Proband 16

Comparative genomic hybridization microarray (Affymetrix, Cytoscan HD) performed at birth revealed a 469 kb deletion at 2q11.2 (GRCh37: 100,235,810–100,704,378) that includes a portion of *AFF3* and was first interpreted as of unknown significance. Other unremarkable laboratory studies included chromosome breakage studies, cerebrospinal fluid (CSF) lactate, methyltetrahydrofolate, and neurotransmitter levels. Trio whole-exome sequencing (GeneDx) ordered at the onset of severe epilepsy confirmed that the partial *AFF3* deletion occurred *de novo* and with no other clinically significant findings except a maternally inherited pathogenic variant in *HEXA* (c.155C>A [p.Ser52*]) (MIM: 606869) that is associated with the autosomal recessive Tay-Sachs disease (MIM: 272800).

Protein alignment and phylogenetic tree

ALF family members' protein sequences were collected from the NCBI database and UCSC Genome Browser, aligned with Clustal Omega³⁰ (v.1.2.4), and imported on Jalview³¹ for visualization. The maximum likelihood phylogenetic tree was based on the Jones-Taylor-Thornton (JTT) model using MEGA X.³² We conducted a bootstrap test with 100 replicates to evaluate the statistical significance of each node.

Interaction modeling

3D modeling for *AFF3* (UniProt: P51826) and *SIAH1* (UniProt: Q8IUQ4) interaction³³ was obtained on Swiss-PdbViewer-DeepView³⁴ v.4.1. Because no structural model for human *SIAH1* ubiquitin-ligase was available, we used mouse ubiquitin ligase structure (PBD: 2AN6), which is 100% conserved with human sequence in the binding region.³⁵

Mouse models

Brain neuroanatomical studies were performed on three 16-week-old male mice in C57BL/6N background with homozygous knockout of *Aff3* (*Laf4*).³⁶ We measured 78 brain parameters across three coronal sections as described³⁷ and analyzed data by using a mixed model and comparing the data to more than 100 wild-type males with a false discovery rate of 1%. Other metabolic and anatomical phenotypes were assessed by the Wellcome Trust Sanger Institute through phenotyping of 6 to 13 homozygous and 7 to 14 heterozygous mice and are available on the International Mouse

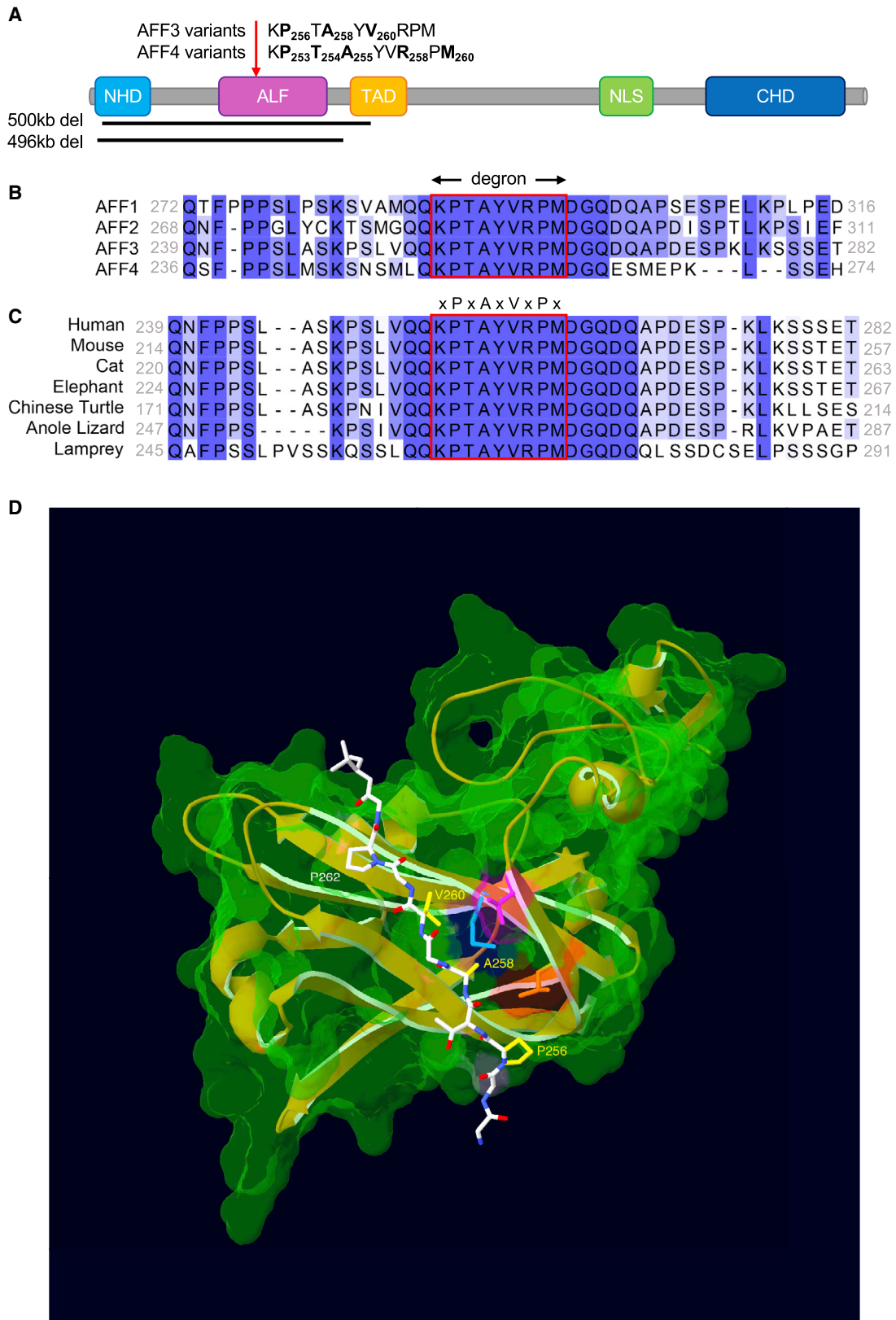


Figure 1. AFF3 and AFF4 degron motif variants

(A) Schematic protein structure of ALF proteins from the amino terminus: an N-terminal homology domain (NHD), the AF4/LAF4/FMR2 (ALF) homology domain²³ containing the SLAH-binding degron motif, a serine-rich transactivation domain (TAD),³ a bipartite nuclear/nucleolar localization sequence (NLS), and a C-terminal homology domain (CHD). The sequences of the degron motifs of AFF3 and AFF4 are shown above. The residues modified in the KINSSHIP probands described in this manuscript and individuals affected by CHOPS^{18,19}

(legend continued on next page)

Phenotyping Consortium website. Engineering of an *Aff3*^{del} mice model carrying a 353 kb deletion homologous to the one harbored by an affected individual¹⁶ was previously published.³⁸ Embryonic day (E) 18.5 animals were processed and stained as described.³⁹ With Taconic Biosciences GmbH (Cologne, Germany), we engineered a constitutive *Aff3*^{A233T} knockin through CRISPR/Cas9-mediated gene editing by using TGGTGGATGCACGCCGGTTA as guide (GenBank: NM_001290814.1 and NP_001277743.1). This allowed the insertion of an additional silent mutation that creates an *AlcI* restriction site for analytical purposes. All procedures were performed in accordance with protocols approved by the local relevant institutional authorities.

Zebrafish overexpression model

Human wild-type open reading frames (ORFs) (*AFF3* [GenBank: NM_002285.2] and *AFF4* [GenBank: NM_014423.4]) cloned into the pEZ-M13 vector were transcribed with the mMESAGE mMESSAGE Kit (Ambion) as prescribed. We injected 1–2 nL of diluted RNA (100–300 ng) inside the yolk, below the cell of wild-type zebrafish embryos at the 1- to 2-cell stage. Phenol red dye with distilled water was injected as vehicle control in similar volume. Injected embryos were raised at 28°C and fixed in 4% paraformaldehyde (PFA) for 2 h at 4–5 days post fertilization (dpf) and stored in PBS at 4°C. Pictures of the embryos were taken after embedding in glycerol. Counts were compared by Fisher's exact test. All procedures were performed in accordance with protocols approved by the veterinary cantonal authority.

Protein accumulation assay

Tagged human wild-type mRNAs cloned into a cytomegalovirus (CMV)-promoted expression vector were obtained from GeneCopoeia. The ORFs of *AFF3* (GenBank: NM_002285.2) were inserted in pEZ-M13 vector with a C-terminal FLAG tag, while the ORF of *SIAH1* (GenBank: NM_001006610) was inserted in pEZ-M07 vector with a C-terminal 3xHA tag. The *AFF3* mutations were engineered with the QuikChange II XL Site-Directed Mutagenesis Kit (Agilent Technologies) following the manufacturer's instructions. HEK293T cells cultured in complete medium (DMEM containing 10% FBS and 1% penicillin-streptomycin) were transiently transfected with wild-type and mutated plasmids with calcium phosphate. 24 h after transfection, medium was changed to fresh

complete medium. Total protein extracts were obtained after 48 h via RIPA buffer with protease and phosphatase inhibitor cocktail. Denatured protein extracts were immunoblotted with anti-FLAG (F3165), anti-FLAG HA (12CA5), and anti-FLAG β -actin (A2066) antibodies from Sigma-Aldrich after SDS-PAGE and/or capillary-based immunoassays via the Jess system from ProteinSimple with antibodies anti-FLAG M2 (affinity-purified F1804) from Sigma-Aldrich, anti-FLAG HA (16B12) from Biogen, and anti-FLAG pan actin (CST4968) from Cell Signaling Technology.

Results

We identified 15 unrelated affected individuals with *de novo* missense variants in the ALF domain of *AFF3* (probands 1–15) (Figure 1A and Table 1) through exome sequencing and data aggregation of multiple laboratories and clinical centers via GeneMatcher.⁴⁰ The six different identified missense variants (Table 1) (1) are not present in the gnomAD⁴¹ (v.2.1.1); (2) are predicted to be deleterious by SIFT,⁴² PROVEAN,⁴³ PolyPhen2,⁴⁴ and MutationTaster2;⁴⁵ (3) are part of the top 1% of all deleterious variants with combined annotation-dependent depletion (CADD) scores over 20; and (4) modify highly conserved amino acids (Figures 1B and 1C). Twelve of these probands carry variants affecting the same codon of exon 6, c.772G>T (p.Ala258Ser) (probands 3–6), c.772G>A (p.Ala258Thr) (probands 7–12), c.773C>T (p.Ala258Val) (probands 13 and 14), whereas probands 1, 2, and 15 carry variants perturbing neighboring codons, c.766C>G (p.Pro256Ala), c.767C>T (p.Pro256Leu), and c.779T>G (p.Val260Gly) (GenBank: NM_001025108.1, NP_001020279.1; Table 1). Another affected individual with what represents a seventh *de novo* c.772G>A (p.Ala258Thr) missense variant was recently reported¹⁷ (Japanese proband). We also identified an individual carrying a *de novo* 469 kb deletion (proband 16) that removes exons 3 to 12 of *AFF3*, which encode part of its N-terminal region, including the ALF and its degon (Figure 1A). An eighteenth individual (historical deletion proband) carrying

are highlighted in bold and numbered. The extent of the 496 kb deletion identified in this work and the extent of the 500 kb deletion previously described³⁸ are indicated by black bars. A red arrow pinpoints the position of the degon motif.

(B) Amino acid sequence alignment of human *AFF1*, *AFF2*, *AFF3*, and *AFF4* proteins (ENSP00000305689, ENSP00000359489, ENSP00000317421, and ENSP00000265343, respectively) showing the highly conserved degon motif (red rectangle) of the ALF homology domain that provides the binding moiety to the *SIAH* ubiquitin-ligase. Sequence alignment was performed with Clustal Omega and edited with Jalview. Shading is proportional to conservation among sequences.

(C) Amino acid sequence alignment of different *AFF3* vertebrate orthologs showing the conservation of the degon motif (red rectangle). Accession numbers are ENSP00000317421 (human), ENSMUSP0000092637 (mouse), ENSFCAP00000024603 (cat), ENSLAFP00000010776 (elephant), ENSPSIP00000007060 (chinese turtle), ENSACAP00000008035 (anole lizard), and ENSPMAP00000008605 (lamprey).

(D) 3D modeling of the binding of human *AFF3* degon to the mouse *Siah* ubiquitin ligase. We downloaded PDB: 2AN6,³⁵ in Swiss-PdbViewer³⁴ and used it as a template to align the human *SIAH* ubiquitin ligase (UniProt: Q8IUQ4).³³ With respect to the mouse crystal structure, the only difference is the presence of an aspartic acid residue instead of a glutamic acid at position 116. We then aligned the region of *AFF3* containing the degon motif (LRPVAMVRPTV) onto the *Siah*-interacting protein⁴⁶ peptide present in the crystal structure (QKPTAYVRPMD) to highlight the position of the variants reported in this study. For clarity, only sidechains of the core degon motif (Pro256, Ala258, Val260, and Pro262) are shown. The sidechains of KINSSHIP mutated residues are highlighted in yellow. The core degon motif adopts a beta-strand conformation directly contacting the ubiquitin ligase-binding groove. The sidechains of Ala258 and Val260 are embedded into binding pockets too small to accommodate larger sidechains.³⁵ They are in direct proximity of *Siah* residues Thr156 (pink) and Met180 (cyan), identified as key binding residues in a series of pull-down assays.³⁵ Replacing Pro256 with Leucine, a residue with a longer sidechain that will be positioned in proximity of *Siah* residue Leu158 (orange), could affect the backbone kink normally conferred by the conserved Proline. The longer sidechains of p.Pro256Leu, p.Ala258Thr, p.Ala258Ser, and p.Ala258Val variants and the smaller p.Pro256Ala and p.Val260Gly are likely to weaken or prevent the interaction with the ligase.

Table 1. Predicted pathogenicity and allele frequencies of *AFF3* de novo missense variants

Gene	Proband	Chromosome coordinates (GRCh37/hg19)	Nucleotide change	Amino acid change	dbSNP (v.152)	GnomAD allele frequency (v.2.1.1)	Deleteriousness prediction (score)				Mutation Taster (19.03.21)
							CADD_PHIRD (GRCh37-v.1.6)	SIFT (v.4.0.3)	PROVEAN (v.1.1)	PolyPhen2 (v.2.2.2)	
<i>AFF3</i>	1	Chr2: 100623276	c.766C>T	p.Pro256Ala	-	0	26.1	damaging (0.000)	deleterious (-6.61)	probably damaging (1.000)	disease causing
NM_001025108.1	2	Chr2: 100623275	c.767C>T	p.Pro256Leu	-	0	27.4	damaging (0.000)	deleterious (-8.26)	probably damaging (1.000)	disease causing
NP_001020279.1	3-6	Chr2: 100623270	c.772G>T	p.Ala258Ser	-	0	24.1	damaging (0.000)	neutral (-2.48)	probably damaging (1.000)	disease causing
7-12 and Japanese proband ¹⁷		Chr2: 100623270	c.772G>A	p.Ala258Thr	rs1131692272	0	23.7	damaging (0.000)	deleterious (-3.30)	probably damaging (1.000)	disease causing
13 and 14		Chr2: 100623269	c.773C>T	p.Ala258Val	-	0	24.1	damaging (0.000)	deleterious (-3.30)	probably damaging (1.000)	disease causing
15		Chr2: 100623263	c.779T>G	p.Val260Gly	-	0	24.2	damaging (0.000)	deleterious (-5.85)	probably damaging (1.000)	disease causing

SIFT cutoff = 0.05, PROVEAN cutoff = -2.5, and PolyPhen2 cutoff = 0.5.

a 500 kb microdeletion and an overlapping phenotype (see below) was also previously described.¹⁶ This deletion removes exons 4 to 13 of *AFF3*³⁸ (Figure 1A).

All missense *AFF3* variants described here and the CHOPS syndrome-associated *AFF4* *de novo* missense variants previously published^{18,19} map within the degron motif of the ALF domain. This highly conserved 9 amino acid sequence [xPxAxVxPx] (Figures 1A and 1B) mediates interaction with SIAH E3 ubiquitin ligases and regulates their degradation.¹ According to pathogenic variant-enriched regions (PERS),⁴⁷ the degron is predicted to be constrained within the ALF family. Pathogenicity of the six *de novo* *AFF3* identified missense variants is further supported by the 3D representation of part of the encoded peptide (Figure 1D). The mutated residues are located within the degron motif (KP₂₅₆TA₂₅₈YV₂₆₀RPM), which adopts a beta-strand conformation directly contacting the SIAH ubiquitin ligase-binding groove.³³ The sidechains of Alanine 258 and Valine 260 are embedded into the hydrophobic core of the beta-sandwich where the binding pockets are too small to accommodate larger sidechains.³⁵ Although the sidechains provided by the p.Pro256Ala and p.Pro256Leu variants would not collide with the Siah residue Leu 158 (Figure 1D), it could affect the backbone kink normally conferred by the conserved Proline at this amino acid position. Thus, variants p.Pro256Ala, p.Pro256Leu, p.Ala258Thr, p.Ala258Ser, p.Ala258Val, and p.Val260Gly are likely to weaken or prevent binding to the ubiquitin ligase. Of note, variants affecting the corresponding Proline 253 and Alanine 255 of *AFF4* (Figure 1A) have been associated with CHOPS syndrome.^{18,19} Hence, all these *de novo* variants, as well as the 496 kb deletion of proband 16 and the previously reported 500 kb deletion¹⁶ that encompass the degron, could result in hindered regulation of *AFF3*.

Consistent with this hypothesis, the *AFF4* *de novo* variants p.Pro253Arg, p.Thr254Ala, p.Thr254Ser, p.Ala255Thr, p.Arg258Trp, and p.Met260Thr that affect its degron motif (KP₂₅₃T₂₅₄A₂₅₅YVR₂₅₈PM₂₆₀) and are associated with CHOPS syndrome (Figure 1A) were shown to be more resistant to degradation upon co-transfection with the SIAH1 ubiquitin ligase.^{18,19} We compared the stability of transiently transfected FLAG-tagged *AFF3*^{wild-type}, *AFF3*^{A258T}, and *AFF3*^{V260G} proteins in presence/absence of HA-tagged SIAH1 E3-ligase and with increasing amount of the MG132 proteasome inhibitor. Notwithstanding testing multiple extraction, separation, and detection methods, we could not observe differences in the stability of the *AFF3* protein variants, suggesting that the degradations of *AFF3* and *AFF4* could be differently regulated (Figures 2A and S1).

We compared the phenotypes of the 16 individuals with missense/deletion variants in *AFF3* described here and those of the two previously reported individuals^{16,17} (Table S1 for detailed phenotypes). While all probands presented with developmental delay/intellectual disability (DD/ID) (18 probands out of 18), some exhibit severe developmental epileptic encephalopathy (14/18), along with

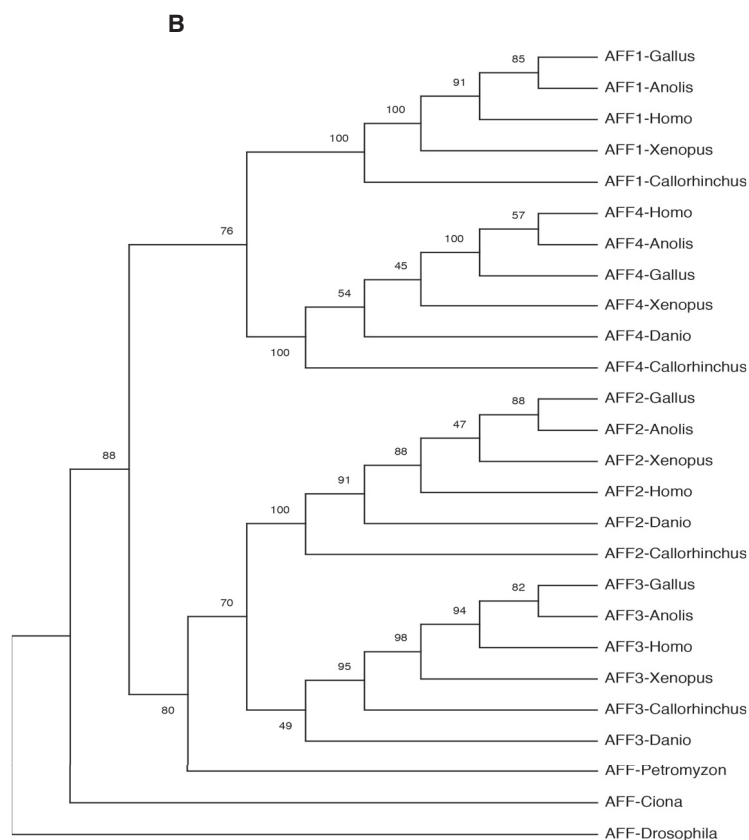
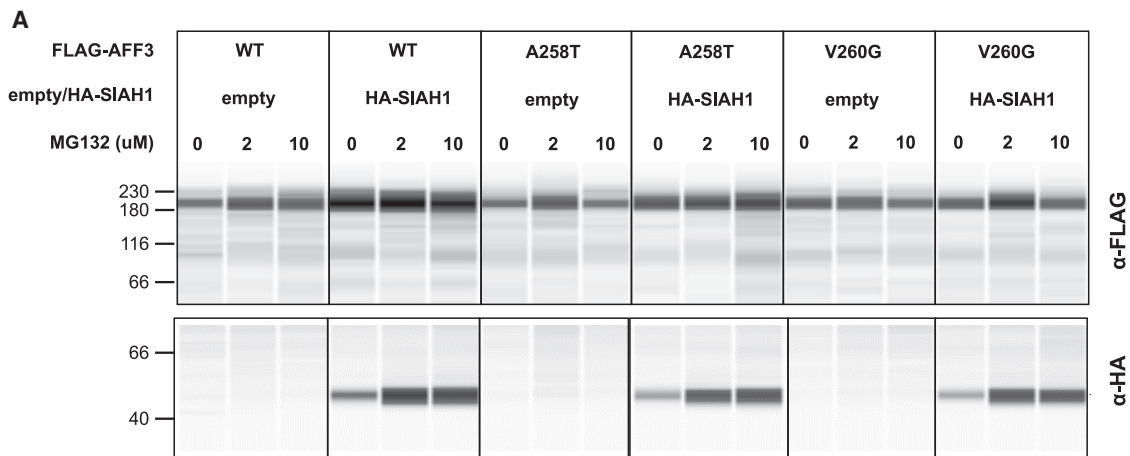


Figure 2. AFF3 stability and evolution

(A) Immunoassays comparing the stability of wild-type and mutated forms of AFF3 proteins. We transiently co-transfected HEK293T cells with expression vectors encoding FLAG-tagged AFF3^{wild-type} (WT), AFF3^{A258T} (A258T), or AFF3^{V260G} (V260G) proteins and HA-tagged SIAH1 E3-ligase (HA-SIAH1) or an empty vector (empty) in presence/absence of increasing amount of the MG132 proteasome inhibitor (0, 2, and 10 μ M). Protein extracts were separated by capillarity on a Jess system and immunoassayed with an anti-FLAG antibody (upper portion) and an anti-HA antibody (bottom portion). The image shows a typical example of eight replicas performed in the same conditions. Loading control and normalization are shown in [Figure S1](#).

(B) ALF protein phylogeny. The maximum likelihood phylogenetic tree was constructed with 26 AFF amino acid sequences: mammals: *Homo sapiens* AFF1 (NP_001160165.1), AFF2 (NP_002016.2), AFF3 (NP_002276.2), and AFF4 (NP_055238.1); birds: *Gallus gallus* AFF1 (XP_004941155.1), AFF2 (XP_015134139.2), AFF3 (XP_015133277.1), and AFF4 (XP_015149549.1); reptiles: *Anolis carolinensis* AFF1 (XP_008109400.2), AFF2 (XP_016851830.1), AFF3 (XP_008118477.1), and AFF4 (XP_003217431.2); amphibians: *Xenopus laevis* AFF1 (XP_018108715.1), AFF2 (XP_018088502.1), AFF3 (XP_018104097.1), and AFF4 (XP_018107624.1); bony fishes: *Danio rerio* AFF2 (XP_002664429.2), AFF3 (XP_021334573.1), and AFF4 (XP_005173956.1); cartilaginous fishes: *Callorhynchus milii* AFF1 (XP_007895125.1), AFF2 (XP_007891068.1), AFF3 (XP_007884050.1), and AFF4 (XP_007889648.1); lamprey: *Petromyzon marinus* AFF (PMZ_0026877); tunicate: *Ciona intestinalis* AFF (XP_018673247.1); and invertebrates: *Drosophila melanogaster* AFF (NP_722863.1). The bootstrap consensus tree inferred from 100 replicates is shown.



Figure 3. Photographs of KINSSHIP-affected individuals with *AFF3* *de novo* missense variants

Proband 4 at 2 years 6 months old (A). Proband 7 at 18 years old (B and I). Proband 8 at 9 months (C) and 21 years old (D and J). Proband 9 at 1 year 7 months (E) and 16 days old (N and O). Proband 10 at 9 years old (F and K–M). Proband 11 at 8 years old (G). Proband 12 at 7 years 9 months old (H and P–R). Proband 15 at 11 years old (S). Note the synophrys and micrognathia, protruding ears, large nose with prominent nasal tip, and prominent teeth in probands 7 (B), 8 (D), 10 (F), and 12 (H), as well as hypertrichosis of the limbs (I, J, M, and P).

(legend continued on next page)

mesomelic dysplasia resembling Nievergelt/Savarirayan mesomelic skeletal dysplasia (NSMSD [MIM: 605274]) (12/18) and failure to thrive (14/18). These features are often associated with microcephaly (9/18), global brain atrophy and/or ventriculomegaly (13/15) (Figure S2), fibular hypoplasia (12/16), horseshoe or hypoplastic kidney (13/17), abnormalities of muscle tone (12/16), gastroesophageal reflux disease (GERD, 6/16), and other gastrointestinal symptoms (14/17). They also share common dysmorphic facial features such as a bulbous nasal tip (10/15), a wide mouth (10/16) often with a square upper lip, abnormalities of the teeth and gums (12/15), and hypertrichosis (12/15) (Figures 3 and 4). Respiratory difficulties/pulmonary involvements were observed in about half of the probands (8/17). Whereas respiratory complications led to the death of proband 7 at 21 years, the historical deletion proband died at 4 months of age after recurrent apneic episodes¹⁶ (Table S1). Consistent with this phenotypic spectrum, common variants in the *AFF3* locus are associated by genome-wide association studies (GWASs) with chronic kidney disease, cognitive ability, GERD, BMI/waist-hip ratio, adolescent idiopathic scoliosis, and vital capacity.⁴⁸

The constellation of features of the affected individuals recalls some features of CHOPS-affected individuals. The three originally described probands,¹⁸ along with the eight later identified,¹⁹ presented with distinctive facial dysmorphic features reminiscent of CdLS, short stature with obesity (11/11), DD/ID (11/11), and microcephaly (6/11) without epilepsy. They showed gastrointestinal abnormalities (8/11) accompanied by abnormal feeding behavior (6/6), hearing loss (8/11), cardiac (8/11) and pulmonary defects (8/11), and rarely horseshoe kidney (2/11). Although they present with vertebral abnormalities (5/11) and brachydactyly (8/11), mesomelic dysplasia is never observed and hypoplastic fibula only rarely (1/11).

Although phenotypes of *AFF3* and *AFF4* missense variant carriers are overlapping, they are not identical. We thus suggest naming the distinct autosomal dominant *AFF3*-associated disorder KINSSHIP syndrome (KI for horseshoe kidney, NS for Nievergelt/Savarirayan type of mesomelic dysplasia, S for seizures, H for hypertrichosis, I for intellectual disability, and P for pulmonary involvement [MIM: 619297]) to evoke its cardinal characteristics, as well as its similarity (common mode of action and inheritance and overlapping phenotypes) to CHOPS syndrome.

To better understand the functional effects of *AFF3* variation, we investigated both knockout and knockin mouse models (Table 2). We first studied the knockout mouse line engineered by the International Mouse Phenotyping Consortium (IMPC).³⁶ The IMPC routinely measures an extensive series of parameters and evaluates whether those are significantly different from wild-type mice⁴⁹ ($p \leq 10^{-4}$).

Aff3^{+/-} and *Aff3*^{-/-} mice exhibit skeletal defects, including fusion of vertebral arches, vertebral transformation, and decreased caudal vertebrae number. Homozygous knockout mice also show an abnormal skull shape with a small, deviated snout and malocclusion as well as decreased serum fructosamine and albumin levels that could reflect kidney defects and/or metabolic dysregulation. Neurological dysfunction was also noted with an increased or absent threshold for auditory brainstem response (signs of hearing impairment) and diminished grip strength. Because *Aff3* is expressed in neural progenitor cells⁵⁰ and required for neuronal migration in the cerebral cortex,⁵¹ we further assessed the consequences of *Aff3* disruption on brain development by measuring a standardized set of 78 parameters across 22 brain regions.³⁷ Compared with wild-type males, homozygous *Aff3*^{-/-}, but not heterozygous *Aff3*^{+/-}, males exhibited significantly enlarged lateral ventricles ($p = 1.24E-4$) and decreased corpus callosum size ($p = 3.02E-6$; Figure 5), similar to the phenotypes observed in multiple probands (Table S1; Figure S2). These features are in stark contrast with results obtained with another engineered *Aff3*^{-/-} line that showed no phenotypic perturbations possibly because of genetic background differences, i.e., C57BL/6N versus CD1, and/or a specific focus on limb morphology.³⁸

We then reassessed mouse models mimicking the deletion identified in the previously described historical deletion proband,¹⁶ which were engineered to test an aggregation method for the rapid generation of structural variants.³⁸ Consistent with the phenotype of both deletion probands, homozygous animals chimeric for a 353 kb deletion syntenic to the 500 kb human deletion exhibited mesomelic dysplasia (12 out of 12 E18.5 embryos; 100%), triangular tibia (12/12), severe hypoplastic fibula (12/12), and polydactyly of the feet (5/12; 42%)³⁸ (Tables 2 and S2). Reexamination of these *Aff3*^{del/del} (*Laf4*^{del/del}) mice at E14.5 and E18.5 showed that they also presented with reduced body size (12 out of 12 E18.5 embryos; 100%), craniofacial dysmorphisms with delayed ossification of skull bones (12/12), hypoplastic pelvis (12/12), intestinal prolapse (10/12; 83%), and neurological dysfunction (12/12) (Figures 6A–6C; Table S2). Chimeric *Aff3*^{del/+} heterozygotes presented with highly variable features ranging from normal phenotypes to homozygous deletion-like phenotypes. Whereas *Aff3*^{del/+} animals with low chimerism were fertile, they produced no heterozygous offspring, suggesting lethality of the 353 kb deletion (Table 2). These results support a causative role of the deletions in the probands phenotypes.

To further assess the underlying mutational mechanism in the missense probands, we engineered a knockin mouse model carrying the *Aff3*^{A233T} mutation that is the

Together with probands 9 and 11, they exhibit thick hair, long eyelashes, and a wide mouth (E and G). Facial features coarsen with age as shown by pictures of proband 8 at different ages (C and D), explaining the more delicate features of younger probands (A and E). *AFF3* *de novo* missense variant carriers also have hypoplastic talipes and abnormalities of toes (I, J, and M–S). Proband 10 also shows clinodactyly and soft tissue syndactyly of both hands (K and L).



Figure 4. X-rays of KINSSHIP-affected individuals with *de novo* missense variants in *AFF3*

(A–D) Proband 7 at 18 years old. Severe scoliosis (A), dorsal and radial bowing of the radius and "V-shaped" proximal carpal bones as seen in Madelung deformity (B), metaphyseal widening and hypoplastic fibula (C), and hypoplastic talipes (D). (E–I) Proband 8 at 21 years old. Static scoliosis (E) and short ulna and radius (F). Note erratic articulation of the styloid process of the ulna on the radius rather than on the carpal bones. Congenital fusion of the bases of the second and third right metatarsals (G), forearm with dislocation of proximal radius (H), and hypoplastic and short bowed tibias with enlarged metaphyses (I). (J–L) Proband 9 at 10 months old. Right foot with 4th and 5th metatarsals synostosis (J) and left foot missing the lateral ray (K) and extremely short rectangular fibula and bowed tibia (L). (M) Proband 11 at 8 years old. Hypoplastic fibula (M). (N–P) Proband 15 at 10 years old. Scoliosis and cervical ribs (N), bowed radius with proximal dislocated head (O), and distal shortening of ulna bowed tibia, severely hypoplastic fibula and oligodactyly (P).

equivalent of the most commonly observed *de novo* missense variant identified in probands 7 to 12 and in the published Japanese proband¹⁷ (p.Ala258Thr). The microinjection of a total of 410 C57BL/6NTac zygotes and transfer into 14 recipient females to allow CRISPR/Cas9 editing resulted in only 13 pups at weaning. Genotyping showed that most of them were either wild type

(8 individuals) or carried CRISPR/Cas9-mediated indels (4), although a reduced guide RNA concentration was used for microinjection. A single female F0 founder animal showed the targeted Ala233Thr knockin but with a very low mosaicism rate of 16.7% in an ear biopsy. Genotyping showed that none of its offspring from four consecutive pregnancies were heterozygous for the mutation. These

Table 2. AFF3 mice models and their phenotypes

Producer	IMPC ^{36, a}		Kraft et al. ³⁸	This work			
Background	C57BL/6N		CD1	CD1		C57BL/6N	
Genotype	<i>Aff3</i> ^{+/-}	<i>Aff3</i> ^{-/-}	<i>Aff3</i> ^{-/-}	<i>Aff3</i> ^{del/+}	<i>Aff3</i> ^{del/del^b}	<i>Aff3</i> ^{A233T}	
Phenotype	Craniofacial anomalies	-	+	N/A	variable features, from non-affected to homozygous-like phenotype	12 out of 12 individuals (100%)	N/A
	Vertebral malformations	+	+	N/A		N/A	
	Mesomelic dysplasia	-	-	-		12 out of 12 individuals (100%) ³⁸	
	Polydactyly	-	-	-		5 out of 12 individuals (42%)	
	Kidney malfunction	-	+	N/A		N/A	
	Intestinal prolapse	-	-	N/A		10 out of 12 individuals (83%)	
	Neurological dysfunctions	-	+	N/A		12 out of 12 individuals (100%)	
	Neuroanatomical defects	N/A	+	N/A		N/A	
	Reduced body size	-	-	N/A		12 out of 12 individuals (100%)	
	Lethality	-	-	N/A	low chimerism, no heterozygous offspring, suggesting lethality	postnatal lethality	no heterozygous offspring, suggesting lethality

^aIMPC significance threshold $p \leq 10E-4$.

^bThe results are shown for E18.5 embryos; these and results for E14.5 are detailed in Table S2.

results suggest that the *Aff3*^{A233T} mutation is lethal at high mosaicism (homozygous *Aff3*^{A233T/A233T} and heterozygous *Aff3*^{+/A233T} chimeras) in gametes or during the fetal period (heterozygous *Aff3*^{+/A233T}; Table 2). The success rate of similar CRISPR/Cas9 knockin projects performed by Taconic Biosciences GmbH (Cologne, Germany) through the years further supports this hypothesis. Out of 92 attempted knockin constructs, 98% were successful and only 2% failed to generate F0 animals. For most of these Taconic projects, positive F1 animals were also generated (A. Reymond, personal communication).

To lend support to the model centered on a pathological increase of AFF3 protein product in affected individuals, we assessed its accumulation in zebrafish independently of any variation. Whereas the genome of these teleosts encodes four ALF transcription factors orthologous to the mammalian *AFF1* to *AFF4*, these genes do not harbor a [xPxAxVxPx] degron motif, suggesting that their degradation is regulated differently in fish. Therefore, we modeled accumulation by independently overexpressing increasing amounts of unmutated human *AFF3* and *AFF4* mRNA in zebrafish embryos. We observed a dose-dependent increase in the fraction of 4 dpf embryos with morphological defects upon overexpression of *AFF3*. The observed phenotypes included bent body axis, yolk sac edema, and generalized body development defects at higher doses (Figures 6D and 6E). A similar albeit less pronounced dose-dependent increase in zebrafish embryos with morphological defects was seen upon overexpression of *AFF4* (Figure 6E).

We then assessed the phylogenesis of the ALF family members. This showed that *AFF2* and *AFF3* are closely related, whereas the branches harboring *AFF1* and *AFF4* cluster together (Figure 2B). The ALF phylogenetic tree suggests two subsequent duplications possibly corresponding to the two full genome duplications that took place early in the vertebrate lineage. The first one split the *AFF2/AFF3* ancestors from the *AFF1/AFF4* precursors, while the second one resulted in the four paralogs we have today. This evolutionary tree also indicates that *AFF2* and *AFF3* could be more functionally redundant than *AFF1* and *AFF4*. This hypothesis is supported by previously published knockdown experiments that assessed the redundancy of ALF transcription factors.⁵² While Luo and colleagues⁵² determined that *AFF2*, *AFF3*, and *AFF4* have mostly different target genes, they also showed that the subset of their common targets were similarly influenced by decreased expression of *AFF2* and *AFF3*, whereas knocking down *AFF3* and *AFF4* had the opposite effect. Within the genes perturbed by both *AFF3* and *AFF4*, we observed a significant overrepresentation of genes implicated in the gastrin hormone pathway (CCKR [cholecystokinin receptor] signaling map, P06959) and a proton pump complex (vacuolar proton-transporting V-type ATPase complex, GO: 0016471) possibly associated with the GERD observed in both KINSSHIP- and CHOPS-affected individuals. Genes linked to the gonadotropin-releasing hormone receptor pathway are similarly enriched (P06664) as targets of *AFF3* and *AFF4*. This observation could be related to the

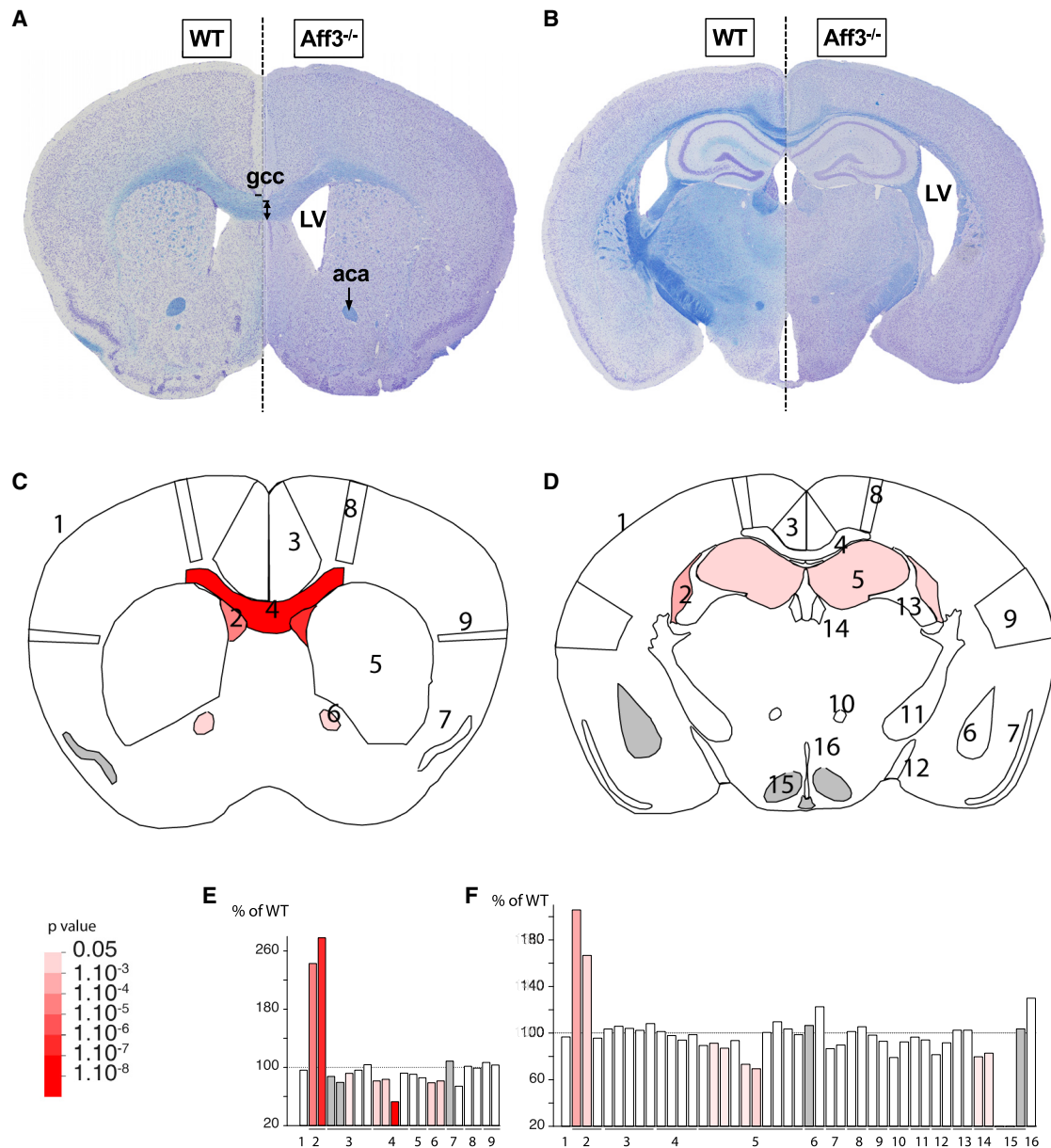


Figure 5. Neuroanatomical defects in *Aff3*^{-/-} mice

(A–F) Merged double-stained sections in *Aff3*^{-/-} mice (right of dashed lines) and their matched controls (WT, wild-type, left of dashed lines) at the striatum (A) and at the hippocampus (B) levels with schematic representation of the affected areas (C and D). Histograms showing the percentage of increase or decrease of parameters in measured areas as compared to the controls for striatum (E) and hippocampus (F) sections. Red shading is proportional to the stringency of the significance threshold. Numbers indicate studied areas: 1, total brain area; 2, lateral ventricles; 3, cingulate cortex (section 1) and retrosplenial cortex (section 2); 4, corpus callosum; 5, caudate putamen (section 1) and hippocampus (section 2); 6, anterior commissure (section 1) and amygdala (section 2); 7, piriform cortex; 8, motor cortex; 9, somatosensory cortex; 10, mammillo-thalamic tract; 11, internal capsule; 12, optic tract; 13, fimbria; 14, habenular; 15, hypothalamus; 16, third ventricle. Results demonstrate an enlargement of lateral ventricles (LVs; $p = 1.24E-4$ on section 1, $p = 4.64E-2$ on section 2) and a smaller genu of the corpus callosum (gcc; decreased corpus callosum size $p = 6.35E-2$ indicated by the black dash and double arrow, decreased bottom width of the corpus callosum $p = 3.02E-6$ and decreased height of the corpus callosum $p = 4.96E-2$). Other phenotypes such as atrophy of the anterior commissure (aca; $p = 1.02E-2$) and smaller hippocampus ($p = 4.02E-2$) are significant if using a less stringent cutoff.

cryptorchidism of KINSSHIP proband 4 and the small genitalia/cryptorchidism in three out of five males affected by CHOPS syndrome,^{18,19} as well as the erratic menstrual cycle of proband 8 (most probands were too young to predict any pubertal anomaly) and popliteal pterygium in proband 11 (Table S1).

Discussion

The eighteen individuals harboring *de novo* *AFF3* variants, either missense in the degtron or deletion encompassing the degtron, described here or in the literature^{16,17} have a complex but recognizable and overlapping clinical

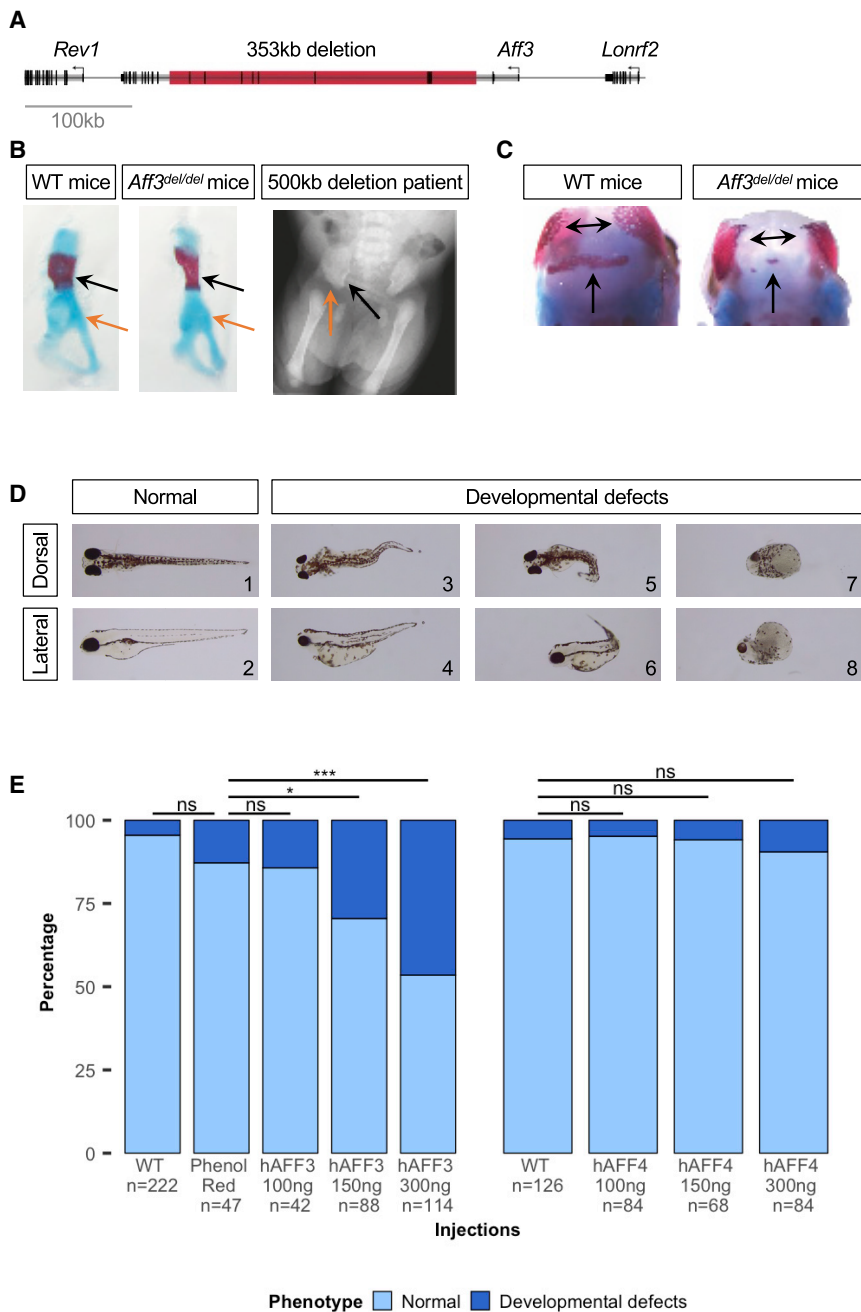


Figure 6. Animal models

(A) Schematic representation of the deletion generated in mice ES cells with the CRISPR/Cas9 system, which models the mutation observed in the historical deletion proband.^{16,38}

(B) Skeletal staining of E18.5 mouse embryos shows mesomelic dysplasia with triangular tibia and hypoplastic fibula (see Figure 3 in Kraft et al.³⁸), as well as a hypoplastic pelvis in *Aff3^{del/del}* mice, especially noticeable in the iliac wing (black arrows) and acetabulum (orange arrows); perturbations also observed in the historical deletion proband.

(C) Delayed ossification of flat bones in the skull of *Aff3^{del/del}* mice.

(D) Lateral (top line) and dorsal (bottom line) views of the observed phenotypes of 4 dpf AB-WT zebrafish embryos injected with human *AFF3* mRNA (hAFF3). hAFF3-injected zebrafish embryos exhibit severe developmental defects, including a bent body axis and yolk sac edema (D3–D6), as well as extreme malformations with absence of body axis, tail, and fins and cyclopia (D7 and D8). Embryos with normal development are displayed for comparison (D1 and D2).

(E) Proportions of normal and developmentally defective 4 dpf AB-WT zebrafish embryos upon injection of increasing doses of hAFF3 (left panel) and hAFF4 (right panel) mRNA. Dark and light colors indicate developmentally defective and normal animals, respectively. Control injections with phenol red show no significant (ns) differences with WT in both *AFF3* and *AFF4* experiments (Fisher's exact test, $p = 0.09$ and $p = 0.12$, respectively). hAFF3 mRNA injection significantly increases the number of zebrafish with developmental defects when compared with controls starting from 150 ng (*; $p = 0.03$) and reinforced at 300 ng (***) ($p = 3.2E-5$). *AFF4* injections do not have a significant impact on zebrafish development compared to WT, even at the same dose (300 ng, $p = 0.29$).

presentation, which we named KINSSHIP syndrome. One of the cardinal characteristics of this rare autosomal dominant syndrome is mesomelic dysplasia with short forearms, radial head dislocation/subluxation, triangular and/or short tibia, fibular hypoplasia, hip dislocation, and tarsal and/or metatarsal synostosis resembling NSMSD (Figure 4). NSMSD is a sporadic or rare autosomal dominant condition^{53,54} associated with neurodevelopmental and often urogenital abnormalities.^{46,55} KINSSHIP-affected individuals similarly present with vertebral and bone mineralization defects, scoliosis, epilepsy, severe global DD/ID sometimes associated with structural brain abnormalities, significant feeding difficulties, horseshoe kidney, hypertrichosis, and distinctive facial features. Multiple

probands showed coarsening of facial features with age, including a large nose with bulbous nasal tip, a prominent columella, and a wide mouth with a square upper lip (Figures 3, 4, and S2; Table S1).

Despite the limited number of individuals, similarities and differences are notable between individuals with KINSSHIP and CHOPS^{18,19,56} syndromes. Individuals with variants in *AFF3* and *AFF4* share features that include respiratory difficulties and vertebral abnormalities, as well as less specific clinical findings such as microcephaly, DD/ID, and GERD. Although skeletal abnormalities are reported in both CHOPS and KINSSHIP syndromes, KINSSHIP-affected individuals present with mesomelic dysplasia, whereas CHOPS-affected individuals show less specific

vertebral anomalies and brachydactyly. Seizures and failure to thrive are more specific to KINSSHIP and obesity to CHOPS. Congenital heart defects and hearing loss are regularly observed in CHOPS (75% of affected individuals versus 18% in KINSSHIP), while kidney abnormalities and hypoplastic fibulae are predominantly present in KINSSHIP syndrome (77% of affected individuals versus 9% in CHOPS). Despite having thick hair and coarse facies in common, CHOPS probands differ from KINSSHIP probands in that their round face and dysmorphic features more closely resemble those of CdLS-affected individuals.^{18,19} Similarly, KINSSHIP-affected individuals presented with a different phenotype than individuals affected with the recently described disease associated with *SIAH1 de novo* variants that encodes the AFF4 E3 ubiquitin ligase. They were affected by developmental delay, hypotonia, laryngomalacia, and GERD but showed no vertebral anomalies, kidney defects, and/or hypoplastic fibulae.⁵⁶ Our results showed no differences in the stability of the proteins encoded by the *AFF3* pathogenic variants, suggesting that the turnover of *AFF3* and *AFF4* could be differently regulated and possibly involve different SIAHs. Support for this notion stems from the remarkable correlation in expression pattern between *SIAH1* and *AFF4* transcripts according to GTEx. All other *AFFs*, in particular *AFF3*, and the other two human *SIAH* paralogs do not show such correlation. Accordingly, *SIAH1* and *SIAH2* (MIM: 602213) have been shown to have different substrates.⁵⁷

Although proteins encoded by *AFF2*, *AFF3*, and *AFF4* were initially reported to be functionally redundant, at least in regulating splicing and transcription during normal brain development,⁵⁸ the clinically distinct phenotypes of individuals carrying *de novo* variants in the degron motifs of *AFF3* and *AFF4* and our zebrafish model results suggest that the encoded proteins are not fully redundant. Further support for this hypothesis is provided by (1) the intolerance to loss-of-function (LoF) variants of *AFF1* (pLI = 0.8), *AFF2* (pLI = 1), *AFF3* (pLI = 1), and *AFF4* (pLI = 1) reported by gnomAD; (2) their different expression patterns according to GTEx; (3) the fact that the majority of their targets are distinct;⁵² and (4) our phylogenetic analysis that indicates that *AFF2* and *AFF3* are more closely related to each other and distinct from *AFF4* (Figure 2B), in line with their similar effects on common targets.⁵²

AFF3 is one of the targets of the Wnt/ β -catenin pathway, an important contributor to pathways involved in bone development and homeostasis.^{59,60} Variants in *WNT* genes cause a diverse range of skeletal dysplasias, including mesomelic defects (*WNT5A*; Robinow syndrome, dominant type [MIM: 180700]), decreased bone density (*WNT1*; osteogenesis imperfecta, type XV [MIM: 615220]), and limb hypoplasia-reduction defects including fibular a/hypoplasia (*WNT3* and *WNT7A*; tetra-amelia [MIM: 273395] and Fuhrmann syndrome [MIM: 228930], respectively). Notably, individuals with Robinow type rhizo/mesomelic dysplasia also present

with developmental kidney abnormalities,⁶¹ whereas perturbations of the Wnt/ β -catenin pathway have been associated with perturbations of the development of ectodermal appendages such as hair and teeth.⁶² Twelve out of fifteen KINSSHIP probands show dental/gum anomalies. Although widespread hypertrichosis may have been partially caused by multi-drug, antiepileptic treatment in some probands, its presence in a non-epileptic *AFF3* individual (proband 13) and the younger proband 9 seems to confirm the association of this feature with *AFF3* genetic variants. It is possible that the complex clinical presentation of the individuals described here (Table S1) may represent the effects of impaired *AFF3* function on a number of downstream targets within the Wnt/ β -catenin pathway. In-depth transcriptome analysis of disease relevant tissues from affected individuals and/or animal models is warranted to confirm this hypothesis.

The pathogenetic mechanism underlying the microdeletion uncovered in the historical deletion proband (Figure 1A) was proposed to act as a dominant negative.³⁸ The predicted structural changes induced by the missense variants identified in the other KINSSHIP-affected individuals (Figure 1D) are likewise consistent with a dominant-negative mode of action. The lethality of the *Aff3*^{A233T} mosaic mice does not refute the hypothesis of a dominant-negative effect because, in these animals, multiple cells were probably homozygous for the mutation. The deleterious effect of not having the correct amount of *AFF3* transcription factor at the appropriate moment and place is further exemplified by our zebrafish overexpression experiments (Figures 6D and 6E) and the phenotypes we observed in heterozygous and homozygous *Aff3*^{-/-} knockout mice^{36,38} (Figure 5 and Table 2). Untimely over- and underexpression could explain the similarities between the phenotypes induced by dominant-negative mutations and loss-of-function variants.

Whereas homozygous *Aff3*^{-/-} knockout mice display features comparable to those presented by KINSSHIP-affected individuals, such as skeletal anomalies, kidney defects, brain malformations, and neurological anomalies, these animals do not recapitulate the distinctive mesomelia in contrast to the *Aff3*^{del/del} mouse model. This result and the aforementioned intolerance to LoF suggest that *AFF3* could be associated with two different syndromes: the one described here caused by missense variants in the degron or hemizygous deletions of the degron and a second one associated with LoF variants for which affected humans remain to be identified. Although this hypothesis warrants further investigation, we have identified by exome sequencing an individual with features partially overlapping those of KINSSHIP. He is compound heterozygous for a truncating mutation and a predicted deleterious missense variant outside of the degron.

In conclusion, we describe a pathology that we propose to name KINSSHIP syndrome. This disorder is associated

with variants that possibly impair the degradation of the encoded protein as they affect the degron motif of AFF3. This syndrome shows partial similarity with the *AFF4*-associated CHOPS syndrome in the type and range of affected tissues and mode of action. However, specific KINSSHIP features such as mesomelic dysplasia, fibular hypoplasia, and horseshoe kidney/renal hypoplasia allow for clear clinical differentiation.

Data and code availability

All datasets and/or code associated with this report are publicly available.

Supplemental information

Supplemental information can be found online at <https://doi.org/10.1016/j.ajhg.2021.04.001>.

Acknowledgments

We thank the probands and their families for their participation in this study. We are grateful to Jacques S. Beckmann, Giedre Grigelioniene, and the Genomic Technologies Facility and the Protein Analysis Facility of the University of Lausanne. This work was supported by grants from the Swiss National Science Foundation (31003A_182632 to A.R.), The Simons Foundation (SFARI274424 to A.R. and SFARI337701 to W.K.C.), the JPB Foundation to W.K.C., the NHGRI (UM1HG007301 to S.M.H., E.M.B., G.M.C.), the Lejeune Foundation to A.R., and the Czech Ministry of Health (17-29423A to Z.S.). The DDD study presents independent research commissioned by the Health Innovation Challenge Fund (HICF-1009-003), a parallel funding partnership between Wellcome and the Department of Health, and the Wellcome Sanger Institute (WT098051). The views expressed in this publication are those of the authors and not necessarily those of Wellcome or the Department of Health. The study has UK Research Ethics Committee approval (10/H0305/83, granted by the Cambridge South REC, and GEN/284/12, granted by the Republic of Ireland REC). The research team acknowledges the support of the National Institute for Health Research through the Comprehensive Clinical Research Network. This study makes use of DECIPHER, which is funded by the Wellcome. We acknowledge the Sanger Mouse Genetics Project for providing mouse samples, funded by the Wellcome Trust (098051). The Australian National Health and Medical Research Council (NHMRC) provided funding for sequencing proband 13 under the Australian Genomics Health Alliance (GNT1113531); the contents are solely the responsibility of the individual authors and do not reflect the views of the NHMRC. The research conducted at the Murdoch Children's Research Institute was supported by the Victorian Government's Operational Infrastructure Support Program. The funders had no role in study design, data collection and analysis, decision to publish, or preparation of the manuscript.

Declaration of interests

T.F., G.D., J.J., L.R., and R.E.S. and W.K.C. are employees and former employees of GeneDx, respectively. The remaining authors declare no competing interests.

Received: July 2, 2019

Accepted: March 29, 2021

Published: May 6, 2021

Web resources

Clustal Omega, <http://www.clustal.org/omega/>
DDD, <https://www.ddduk.org/>
GeneDx ClinVar submission page, <https://www.ncbi.nlm.nih.gov/clinvar/submitters/26957/>
GeneMatcher, <https://genematcher.org/>
gnomAD, <https://gnomad.broadinstitute.org/>
GTEx, <https://www.gtexportal.org/home/>
GWAS Catalog, <https://www.ebi.ac.uk/gwas/>
IMPC, <https://www.mousephenotype.org/>
MutationTaster2, <http://www.mutationtaster.org/>
OMIM, <https://omim.org>
PANTHER, <http://www.pantherdb.org>
PER viewer, <http://per.broadinstitute.org/>
PolyPhen-2, <http://genetics.bwh.harvard.edu/pph2/index.shtml>
PROVEAN, <http://provean.jcvi.org/index.php>
SIFT, <http://provean.jcvi.org>
VarAFT, <https://varaft.eu>
Varapp, <https://varapp-demo.vital-it.ch>

References

1. House, C.M., Frew, I.J., Huang, H.L., Wiche, G., Traficante, N., Nice, E., Catimel, B., and Bowtell, D.D. (2003). A binding motif for Siah ubiquitin ligase. *Proc. Natl. Acad. Sci. USA* *100*, 3101–3106.
2. Bitoun, E., and Davies, K.E. (2005). The robotic mouse: unravelling the function of AF4 in the cerebellum. *Cerebellum* *4*, 250–260.
3. Meyer, C., Hofmann, J., Burmeister, T., Gröger, D., Park, T.S., Emerenciano, M., Pombo de Oliveira, M., Renneville, A., Villarese, P., Macintyre, E., et al. (2013). The MLL recombinome of acute leukemias in 2013. *Leukemia* *27*, 2165–2176.
4. Nilson, I., Reichel, M., Ennas, M.G., Greim, R., Knörr, C., Siegler, G., Greil, J., Fey, G.H., and Marschalek, R. (1997). Exon/intron structure of the human AF-4 gene, a member of the AF-4/LAF-4/FMR-2 gene family coding for a nuclear protein with structural alterations in acute leukaemia. *Br. J. Haematol.* *98*, 157–169.
5. Oliver, P.L., Bitoun, E., Clark, J., Jones, E.L., and Davies, K.E. (2004). Mediation of Af4 protein function in the cerebellum by Siah proteins. *Proc. Natl. Acad. Sci. USA* *101*, 14901–14906.
6. Chen, Y., and Cramer, P. (2019). Structure of the super-elongation complex subunit AFF4 C-terminal homology domain reveals requirements for AFF homo- and heterodimerization. *J. Biol. Chem.* *294*, 10663–10673.
7. Luo, Z., Lin, C., and Shilatifard, A. (2012). The super elongation complex (SEC) family in transcriptional control. *Nat. Rev. Mol. Cell Biol.* *13*, 543–547.
8. Jonkers, I., and Lis, J.T. (2015). Getting up to speed with transcription elongation by RNA polymerase II. *Nat. Rev. Mol. Cell Biol.* *16*, 167–177.
9. Tang, A.H., Neufeld, T.P., Rubin, G.M., and Müller, H.A. (2001). Transcriptional regulation of cytoskeletal functions and segmentation by a novel maternal pair-rule gene, *lilliputian*. *Development* *128*, 801–813.

10. Wittwer, F., van der Straten, A., Keleman, K., Dickson, B.J., and Hafen, E. (2001). Lilliputian: an AF4/FMR2-related protein that controls cell identity and cell growth. *Development* 128, 791–800.
11. Gecz, J., Gedeon, A.K., Sutherland, G.R., and Mulley, J.C. (1996). Identification of the gene FMR2, associated with FRAXE mental retardation. *Nat. Genet.* 13, 105–108.
12. Metsu, S., Rooms, L., Rainger, J., Taylor, M.S., Bengani, H., Wilson, D.I., Chilamakuri, C.S., Morrison, H., Vandeweyer, G., Reyniers, E., et al. (2014). FRA2A is a CGG repeat expansion associated with silencing of AFF3. *PLoS Genet.* 10, e1004242.
13. Luo, Z., Lin, C., Woodfin, A.R., Bartom, E.T., Gao, X., Smith, E.R., and Shilatifard, A. (2016). Regulation of the imprinted Dlk1-Dio3 locus by allele-specific enhancer activity. *Genes Dev.* 30, 92–101.
14. Wang, Y., Shen, Y., Dai, Q., Yang, Q., Zhang, Y., Wang, X., Xie, W., Luo, Z., and Lin, C. (2017). A permissive chromatin state regulated by ZFP281-AFF3 in controlling the imprinted Meg3 polycistron. *Nucleic Acids Res.* 45, 1177–1185.
15. Zhang, Y., Wang, C., Liu, X., Yang, Q., Ji, H., Yang, M., Xu, M., Zhou, Y., Xie, W., Luo, Z., et al. (2018). AFF3-DNA methylation interplay in maintaining the mono-allelic expression pattern of XIST in terminally differentiated cells. *J. Mol. Cell. Biol.* 11, 761–769.
16. Steichen-Gersdorf, E., Gassner, I., Superti-Furga, A., Ullmann, R., Stricker, S., Klopocki, E., and Mundlos, S. (2008). Triangular tibia with fibular aplasia associated with a microdeletion on 2q11.2 encompassing LAF4. *Clin. Genet.* 74, 560–565.
17. Shimizu, D., Sakamoto, R., Yamoto, K., Saito, H., Fukami, M., Nishimura, G., and Ogata, T. (2019). De novo AFF3 variant in a patient with mesomelic dysplasia with foot malformation. *J. Hum. Genet.* 64, 1041–1044.
18. Izumi, K., Nakato, R., Zhang, Z., Edmondson, A.C., Noon, S., Dulik, M.C., Rajagopalan, R., Venditti, C.P., Gripp, K., Samanich, J., et al. (2015). Germline gain-of-function mutations in AFF4 cause a developmental syndrome functionally linking the super elongation complex and cohesin. *Nat. Genet.* 47, 338–344.
19. Raible, S.E., Mehta, D., Bettale, C., Fiordaliso, S., Kaur, M., Medne, L., Rio, M., Haan, E., White, S.M., Cusmano-Ozog, K., et al. (2019). Clinical and molecular spectrum of CHOPS syndrome. *Am. J. Med. Genet. A.* 179, 1126–1138.
20. Urano, A., Endoh, M., Wada, T., Morikawa, Y., Itoh, M., Kataoka, Y., Taki, T., Akazawa, H., Nakajima, H., Komuro, I., et al. (2005). Infertility with defective spermiogenesis in mice lacking AF5q31, the target of chromosomal translocation in human infant leukemia. *Mol. Cell. Biol.* 25, 6834–6845.
21. Deciphering Developmental Disorders, S.; and Deciphering Developmental Disorders Study (2015). Large-scale discovery of novel genetic causes of developmental disorders. *Nature* 519, 223–228.
22. Retterer, K., Juusola, J., Cho, M.T., Vitazka, P., Millan, F., Gibellini, F., Vertino-Bell, A., Smaoui, N., Neidich, J., Monaghan, K.G., et al. (2016). Clinical application of whole-exome sequencing across clinical indications. *Genet. Med.* 18, 696–704.
23. Alfaiz, A.A., Micale, L., Mandriani, B., Augello, B., Pellico, M.T., Chrast, J., Xenarios, I., Zelante, L., Merla, G., and Raymond, A. (2014). TBC1D7 mutations are associated with intellectual disability, macrocrania, patellar dislocation, and celiac disease. *Hum. Mutat.* 35, 447–451.
24. Delafontaine, J., Masselot, A., Liechti, R., Kuznetsov, D., Xenarios, I., and Pradervand, S. (2016). Varapp: A reactive web-application for variants filtering. *bioRxiv.* <https://doi.org/10.1101/060806>.
25. Holla, O.L., Bock, G., Busk, O.L., and Isfoss, B.L. (2014). Familial visceral myopathy diagnosed by exome sequencing of a patient with chronic intestinal pseudo-obstruction. *Endoscopy* 46, 533–537.
26. Bowling, K.M., Thompson, M.L., Amaral, M.D., Finnila, C.R., Hiatt, S.M., Engel, K.L., Cochran, J.N., Brothers, K.B., East, K.M., Gray, D.E., et al. (2017). Genomic diagnosis for children with intellectual disability and/or developmental delay. *Genome Med.* 9, 43.
27. Takenouchi, T., Yamaguchi, Y., Tanikawa, A., Kosaki, R., Okano, H., and Kosaki, K. (2015). Novel overgrowth syndrome phenotype due to recurrent de novo PDGFRB mutation. *J. Pediatr.* 166, 483–486.
28. Richards, S., Aziz, N., Bale, S., Bick, D., Das, S., Gastier-Foster, J., Grody, W.W., Hegde, M., Lyon, E., Spector, E., et al.; ACMG Laboratory Quality Assurance Committee (2015). Standards and guidelines for the interpretation of sequence variants: a joint consensus recommendation of the American College of Medical Genetics and Genomics and the Association for Molecular Pathology. *Genet. Med.* 17, 405–424.
29. Sadedin, S.P., Dashnow, H., James, P.A., Bahlo, M., Bauer, D.C., Lonie, A., Lunke, S., Macciocia, I., Ross, J.P., Siemering, K.R., et al.; Melbourne Genomics Health Alliance (2015). Cpipeline: a shared variant detection pipeline designed for diagnostic settings. *Genome Med.* 7, 68.
30. Sievers, F., Wilm, A., Dineen, D., Gibson, T.J., Karplus, K., Li, W., Lopez, R., McWilliam, H., Remmert, M., Söding, J., et al. (2011). Fast, scalable generation of high-quality protein multiple sequence alignments using Clustal Omega. *Mol. Syst. Biol.* 7, 539.
31. Waterhouse, A.M., Procter, J.B., Martin, D.M., Clamp, M., and Barton, G.J. (2009). Jalview Version 2—a multiple sequence alignment editor and analysis workbench. *Bioinformatics* 25, 1189–1191.
32. Kumar, S., Stecher, G., Li, M., Niyaz, C., and Tamura, K. (2018). MEGA X: Molecular Evolutionary Genetics Analysis across Computing Platforms. *Mol. Biol. Evol.* 35, 1547–1549.
33. Santelli, E., Leone, M., Li, C., Fukushima, T., Preece, N.E., Olson, A.J., Ely, K.R., Reed, J.C., Pellicchia, M., Liddington, R.C., and Matsuzawa, S. (2005). Structural analysis of Siah1-Siah-interacting protein interactions and insights into the assembly of an E3 ligase multiprotein complex. *J. Biol. Chem.* 280, 34278–34287.
34. Johansson, M.U., Zoete, V., Michielin, O., and Guex, N. (2012). Defining and searching for structural motifs using DeepView/Swiss-PdbViewer. *BMC Bioinformatics* 13, 173.
35. House, C.M., Hancock, N.C., Möller, A., Cromer, B.A., Fedorov, V., Bowtell, D.D., Parker, M.W., and Polekhina, G. (2006). Elucidation of the substrate binding site of Siah ubiquitin ligase. *Structure* 14, 695–701.
36. Skarnes, W.C., Rosen, B., West, A.P., Koutourakis, M., Bushell, W., Iyer, V., Mujica, A.O., Thomas, M., Harrow, J., Cox, T., et al. (2011). A conditional knockout resource for the genome-wide study of mouse gene function. *Nature* 474, 337–342.
37. Mikhaleva, A., Kannan, M., Wagner, C., and Yalcin, B. (2016). Histomorphological Phenotyping of the Adult Mouse Brain. *Curr. Protoc. Mouse Biol.* 6, 307–332.
38. Kraft, K., Geuer, S., Will, A.J., Chan, W.L., Paliou, C., Borschiwer, M., Harabula, I., Wittler, L., Franke, M., Ibrahim,

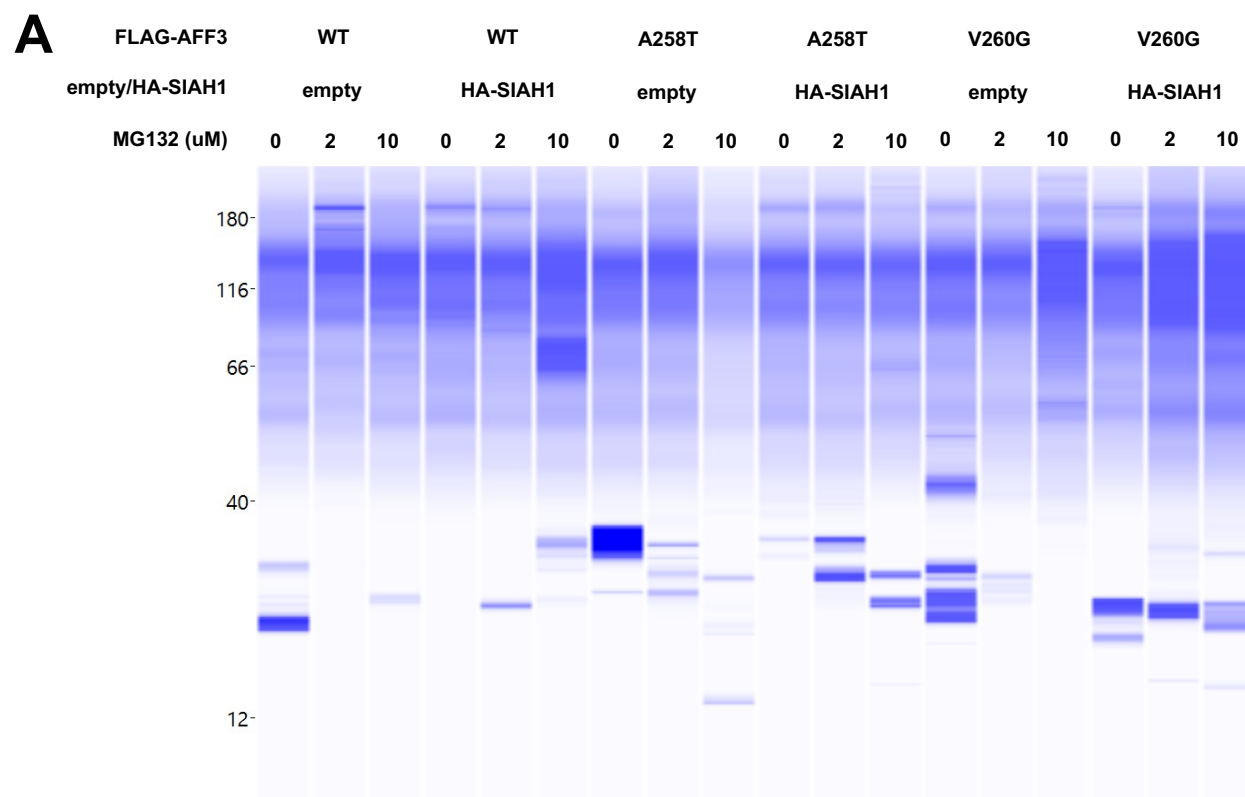
- D.M., et al. (2015). Deletions, Inversions, Duplications: Engineering of Structural Variants using CRISPR/Cas in Mice. *Cell Rep.* 10, 833–839.
39. Mundlos, S. (2000). Skeletal morphogenesis. *Methods Mol. Biol.* 136, 61–70.
 40. Sobreira, N., Schiettecatte, F., Valle, D., and Hamosh, A. (2015). GeneMatcher: a matching tool for connecting investigators with an interest in the same gene. *Hum. Mutat.* 36, 928–930.
 41. Karczewski, K.J., Francioli, L.C., Tiao, G., Cummings, B.B., Alföldi, J., Wang, Q., Collins, R.L., Laricchia, K.M., Ganna, A., Birnbaum, D.P., et al.; Genome Aggregation Database Consortium (2020). The mutational constraint spectrum quantified from variation in 141,456 humans. *Nature* 581, 434–443.
 42. Kumar, P., Henikoff, S., and Ng, P.C. (2009). Predicting the effects of coding non-synonymous variants on protein function using the SIFT algorithm. *Nat. Protoc.* 4, 1073–1081.
 43. Choi, Y., and Chan, A.P. (2015). PROVEAN web server: a tool to predict the functional effect of amino acid substitutions and indels. *Bioinformatics* 31, 2745–2747.
 44. Adzhubei, I.A., Schmidt, S., Peshkin, L., Ramensky, V.E., Gerasimova, A., Bork, P., Kondrashov, A.S., and Sunyaev, S.R. (2010). A method and server for predicting damaging missense mutations. *Nat. Methods* 7, 248–249.
 45. Schwarz, J.M., Cooper, D.N., Schuelke, M., and Seelow, D. (2014). MutationTaster2: mutation prediction for the deep-sequencing age. *Nat. Methods* 11, 361–362.
 46. Tüysüz, B., Zeybek, C., Zorer, G., Sipahi, O., and Ungür, S. (2002). Patient with the mesomelic dysplasia, Nievergelt syndrome, and cerebellovermian agenesis and cataracts. *Am. J. Med. Genet.* 109, 206–210.
 47. Pérez-Palma, E., May, P., Iqbal, S., Niestroj, L.M., Du, J., Heyne, H.O., Castrillon, J.A., O'Donnell-Luria, A., Nürnberg, P., Palotie, A., et al. (2020). Identification of pathogenic variant enriched regions across genes and gene families. *Genome Res.* 30, 62–71.
 48. Buniello, A., MacArthur, J.A.L., Cerezo, M., Harris, L.W., Hayhurst, J., Malangone, C., McMahon, A., Morales, J., Mountjoy, E., Sollis, E., et al. (2019). The NHGRI-EBI GWAS Catalog of published genome-wide association studies, targeted arrays and summary statistics 2019. *Nucleic Acids Res.* 47 (D1), D1005–D1012.
 49. Brown, S.D., and Moore, M.W. (2012). The International Mouse Phenotyping Consortium: past and future perspectives on mouse phenotyping. *Mamm. Genome* 23, 632–640.
 50. Fietz, S.A., Lachmann, R., Brandl, H., Kircher, M., Samusik, N., Schröder, R., Lakshmanaperumal, N., Henry, I., Vogt, J., Riehn, A., et al. (2012). Transcriptomes of germinal zones of human and mouse fetal neocortex suggest a role of extracellular matrix in progenitor self-renewal. *Proc. Natl. Acad. Sci. USA* 109, 11836–11841.
 51. Moore, J.M., Oliver, P.L., Finelli, M.J., Lee, S., Lickiss, T., Molnár, Z., and Davies, K.E. (2014). *Laf4/Aff3*, a gene involved in intellectual disability, is required for cellular migration in the mouse cerebral cortex. *PLoS ONE* 9, e105933.
 52. Luo, Z., Lin, C., Guest, E., Garrett, A.S., Mohaghegh, N., Swanson, S., Marshall, S., Florens, L., Washburn, M.P., and Shilatifard, A. (2012). The super elongation complex family of RNA polymerase II elongation factors: gene target specificity and transcriptional output. *Mol. Cell. Biol.* 32, 2608–2617.
 53. Nakamura, M., Matsuda, Y., Higo, M., and Nishimura, G. (2007). A family with an autosomal dominant mesomelic dysplasia resembling mesomelic dysplasia Savarirayan and Nievergelt types. *Am. J. Med. Genet. A.* 143A, 2079–2081.
 54. Bonafe, L., Cormier-Daire, V., Hall, C., Lachman, R., Mortier, G., Mundlos, S., Nishimura, G., Sangiorgi, L., Savarirayan, R., Sillence, D., et al. (2015). Nosology and classification of genetic skeletal disorders: 2015 revision. *Am. J. Med. Genet. A.* 167A, 2869–2892.
 55. Savarirayan, R., Cormier-Daire, V., Curry, C.J., Nashelsky, M.B., Rappaport, V., Rimoin, D.L., and Lachman, R.S. (2000). New mesomelic dysplasia with absent fibulae and triangular tibiae. *Am. J. Med. Genet.* 94, 59–63.
 56. Buratti, J., Ji, L., Keren, B., Lee, Y., Booke, S., Erdin, S., Kim, S.Y., Palculict, T.B., Meiner, V., Chae, J.H., et al. (2021). De novo variants in *SLAH1*, encoding an E3 ubiquitin ligase, are associated with developmental delay, hypotonia and dysmorphic features. *J. Med. Genet.* 58, 205–212.
 57. Gopalsamy, A., Hagen, T., and Swaminathan, K. (2014). Investigating the molecular basis of Siah1 and Siah2 E3 ubiquitin ligase substrate specificity. *PLoS ONE* 9, e106547.
 58. Melko, M., Douguet, D., Bensaid, M., Zongaro, S., Verheggen, C., Gecz, J., and Bardoni, B. (2011). Functional characterization of the AFF (AF4/FMR2) family of RNA-binding proteins: insights into the molecular pathology of FRAXE intellectual disability. *Hum. Mol. Genet.* 20, 1873–1885.
 59. Lefèvre, L., Omeiri, H., Drougat, L., Hantel, C., Giraud, M., Val, P., Rodriguez, S., Perlemoine, K., Blugeon, C., Beuschlein, F., et al. (2015). Combined transcriptome studies identify AFF3 as a mediator of the oncogenic effects of β -catenin in adrenocortical carcinoma. *Oncogenesis* 4, e161.
 60. Zhong, Z., Ethen, N.J., and Williams, B.O. (2014). WNT signaling in bone development and homeostasis. *Wiley Interdiscip. Rev. Dev. Biol.* 3, 489–500.
 61. Tufan, F., Cefle, K., Türkmen, S., Türkmen, A., Zorba, U., Dursun, M., Oztürk, S., Palandüz, S., Ecder, T., Mundlos, S., and Horn, D. (2005). Clinical and molecular characterization of two adults with autosomal recessive Robinow syndrome. *Am. J. Med. Genet. A.* 136, 185–189.
 62. Kimura, R., Watanabe, C., Kawaguchi, A., Kim, Y.I., Park, S.B., Maki, K., Ishida, H., and Yamaguchi, T. (2015). Common polymorphisms in *WNT10A* affect tooth morphology as well as hair shape. *Hum. Mol. Genet.* 24, 2673–2680.

Supplemental information

**Variants in the degron of AFF3 are associated with
intellectual disability, mesomelic dysplasia,
horseshoe kidney, and epileptic encephalopathy**

Norine Voisin, Rhonda E. Schnur, Sofia Douzgou, Susan M. Hiatt, Cecilie F. Rustad, Natasha J. Brown, Dawn L. Earl, Boris Keren, Olga Levchenko, Sinje Geuer, Sarah Verheyen, Diana Johnson, Yuri A. Zarate, Miroslava Hancárová, David J. Amor, E. Martina Bebin, Jasmin Blatterer, Alfredo Brusco, Gerarda Cappuccio, Joel Charrow, Nicolas Chatron, Gregory M. Cooper, Thomas Courtin, Elena Dadali, Julien Delafontaine, Ennio Del Giudice, Martine Doco, Ganka Douglas, Astrid Eisenkölbl, Tara Funari, Giuliana Giannuzzi, Ursula Gruber-Sedlmayr, Nicolas Guex, Delphine Heron, Øystein L. Holla, Anna C.E. Hurst, Jane Juusola, David Kronn, Alexander Lavrov, Crystle Lee, Séverine Lorrain, Else Merckoll, Anna Mikhaleva, Jennifer Norman, Sylvain Pradervand, Darina Prchalová, Lindsay Rhodes, Victoria R. Sanders, Zdeněk Sedláček, Heidelis A. Seebacher, Elizabeth A. Sellars, Fabio Sirchia, Toshiki Takenouchi, Akemi J. Tanaka, Heidi Taska-Tench, Elin Tønne, Kristian Tveten, Giuseppina Vitiello, Markéta Vlčková, Tomoko Uehara, Caroline Nava, Binnaz Yalcin, Kenjiro Kosaki, Dian Donnai, Stefan Mundlos, Nicola Brunetti-Pierri, Wendy K. Chung, and Alexandre Reymond

Figure S1



B

Sample	Primary	PN (%)
AFF3 WT + empty	Flag M2- SLCD3990	100
AFF3 WT +empty + MG132 -2	Flag M2- SLCD3990	103
AFF3 WT +empty + MG132 -10	Flag M2- SLCD3990	104
AFF3 WT +SIAH	Flag M2- SLCD3990	107
AFF3 WT +SIAH + MG132-2	Flag M2- SLCD3990	103
AFF3 WT +SIAH + MG132-10	Flag M2- SLCD3990	117
AFF3 A258T +empty	Flag M2- SLCD3990	104
AFF3 A258T +empty + MG132 -2	Flag M2- SLCD3990	104
AFF3 A258T +empty + MG132 -10	Flag M2- SLCD3990	84
AFF3 A258T +SIAH	Flag M2- SLCD3990	102
AFF3 A258T +SIAH + MG132-2	Flag M2- SLCD3990	101
AFF3 A258T +SIAH + MG132-10	Flag M2- SLCD3990	99
AFF3 V260G +empty	Flag M2- SLCD3990	110
AFF3 V260G +empty + MG132 -2	Flag M2- SLCD3990	100
AFF3 V260G +empty + MG132 -10	Flag M2- SLCD3990	114
AFF3 V260G +SIAH	Flag M2- SLCD3990	103
AFF3 V260G +SIAH + MG132 -2	Flag M2- SLCD3990	122
AFF3 V260G +SIAH + MG132 -10	Flag M2- SLCD3990	124

Figure S1: Loading control and normalization of the FLAG immuno-assays presented in Figure 2A. Protein extracts were separated by capillarity on a Jess system and immuno-assayed with an anti-FLAG antibody. (A) Fluorochrome fixation for normalisation of protein extracts of the Jess run. (B) Normalisation values of all samples in percent (PN) using as reference the protein extract FLAG-AFF3 WT and empty vector.

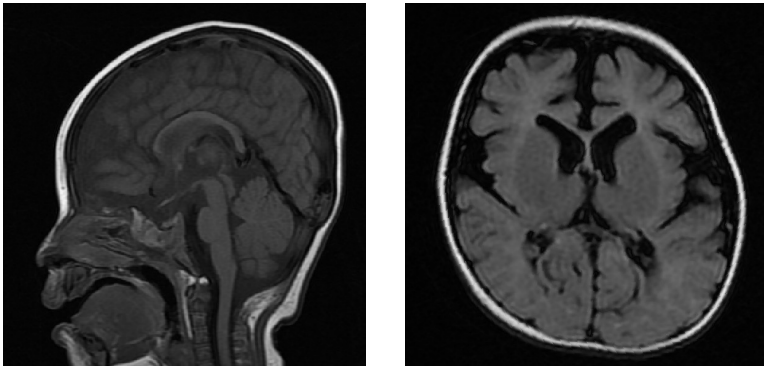


Figure S2: Brain MRI of proband 11 carrying a *de novo* variant in *AFF3*. FLAIR (right) and T1 (left) at 9 months old are shown.

Table S2: Phenotypes of Aff3del/del homozygous in-frame truncation (chimeric mice from diploid aggregation with homozygous ES cells)

phenotype	E18.5		E14.5		E14.5/E18.5 combined	
	numbers	pct[%]	numbers	pct[%]	numbers	pct[%]
polydactyly	5	42	1	25	6	38
mesomelic dyplasia	12	100	4	100	16	100
triangular tibia	12	100	4	100	16	100
hypoplastic fibula	12	100	4	100	16	100
hypoplastic pelvis	12	100	NA		NA	
craniofacial dysmorphism	12	100	4	100	16	100
delayed ossification (skull)	12	100	NA		NA	
intestinal prolapse	10	83	NA		NA	
lack of motoric reflexes /neurological dysfunction	12	100	NA		NA	
reduces body size	12	100	4	100	16	100
abort	1	8	0	0	1	6
total numbers of fetuses (abort excluded)	12	100	4	100	16	100
total numbers of litters	3		1		4	

motoric reflex = touch triggers contraction in E18.5

NA = not available, not investigated, in case of motoric reflexes not applicable